Theoretical Chemistry Accounts manuscript No.
(will be inserted by the editor)

Hirshfeld-I charges in Linear Combination of Atomic Orbitals periodic calculations

C. M. Zicovich-Wilson · M. Hô · A. M. Navarrete-López · S. Casassa

Received: date / Accepted: date

Abstract Hirshfeld-I charges were implemented in the CRYSTAL code, for periodic calculations with localized atomic basis sets. Some particular features of the present periodic implementation are detailed and discussed by means of selected illustrating examples. In these examples, the Hirshfeld-I charges are somewhere between the Bader and the Mulliken values and closer to the former. The implementation exploits heavily symmetry aspects and is shown to scale linearly with the unit cell dimension.

Keywords Hirshfeld Iterative · Periodic calculations · Ab Initio · LCAO

To A. Vela for his high human and scientific qualities.

C. M. Zicovich-Wilson
Centro de Investigación en Ciencias-(IICBA)
Universidad Autónoma del Estado de Morelos
Cuernavaca, Morelos, 62209, México
E-mail: claudio@uaem.mx
Corresponding author

M. Hô
Centro de Investigaciones Químicas
Universidad Autónoma del Estado de Morelos
Av. Universidad 1001, Col. Chamilpa
Cuernavaca, Morelos, 62209, México

A. M. Navarrete-López
Departamento de Química, División de Ciencias Básicas
e Ingeniería, Universidad Autónoma Metropolitana-Iztapalapa
San Rafael Atlixco 186, Col. Vicentina, Iztapalapa C. P. 09340
Ciudad de México, México

S. Casassa
Dipartimento di Chimica, Università di Torino and NIS
Nanostructured Interfaces and Surfaces, Centre of
Excellence, Via Giuria 5, 10125 Torino, Italy

1 Introduction

Ab initio quantum mechanical calculation of periodic systems, which were largely started in the late 70s to early 80s, can be viewed as an extension to molecular systems simulation.[1] Implemented methods tipically differ in their use: plane-wave or atomic centered gaussian functions as basis sets and density functional or wave-function approaches. In principle, a crystal structure consists of a large number ($\approx 10^{20}$) of atoms, a fact that poses a formidable task in the design of codes for electronic structure calculations of these systems. The problem is rendered tractable by: imposing the translational invariance of the lattice in an infinite model and working within periodic boundary conditions. In other words, exploiting the Bloch function approach which allows one-electron wave-functions to be expressed as wave-like parts times periodic functions.

As calculations of periodic systems are a kind of logical continuation of those for molecular systems, so are corresponding properties such as cohesive energy, phase stability, 1- and 2-electron properties, to name a few. Atomic charge represents one of the most popular analysis of the electronic density. Since it is not an observable, various schemes have been developed to partition the whole electronic structure into its atomic fragments. These schemes are generally divided into two classes depending on whether they are based on molecular orbitals or electron density. The most popular method of the first class is the Mulliken equi-partitioned one [2] which depends on the density $\mathbf{P}$ and overlap $\mathbf{S}$ matrices. On the other hand, Löwdin [3] analysis is similar but deals with symmetrically orthogonalized AOs through the $\mathbf{S}^{-1/2}$ transformation. The Natural Bond Orbital [4] method evaluates atomic charges based on rotated molecular orbitals that best resembles localized bonds and lone pairs. Stone's multipole analysis [5] atributes atomic density to contributions from multipole expansion.

The second class is based directly on the electron density $\rho(\mathbf{r})$. Among these are the Voronoi Deformation Density [6] in which atomic *cell* contains regions that are nearest to a particular nucleus, and its improvement by Becke [7] in which atomic density smooths out the Voronoi boundaries by including Becke's weight functions. Bader's QTAIM (*Quantum Theory of Atoms in Molecules*) [8], one of the most rigorous and hence one of the most cost intensive partition scheme, defines atomic basins as those surrounded by *zero-flux surfaces*.

Most notably recently is the work of Hirshfeld-I (HI) method [9] which belongs to the latter class and has renewed interest in the original Hirshfeld scheme. [10] In particular efforts have been made to include open shell algorithms such as the Fractional Occupation HI (FOHI) [11,12] where both spin and atomic charges of spherical atomic densities are optimized independently. In the FOHI method, the spherical atomic densities are obtained by the equi-distribution of the occupation number of valence obitals. In order to eliminate the need of calculating the pro-molecular density and their charged analogues, the Iterative Stockholder Atoms method [13–15] replaces these densities by spherical symmetric weight functions which are in fact spherical averages of the atomic density obtained from a previous step. The iterative process halts when both the atomic charges and the aforementioned spherically averaged densities are solved simultaneously.

As concerns the periodic extension of such approaches, the Mulliken analysis has been one of the earliest methods implemented in *ab initio* public codes in the context of localized basis sets.[1] In 1994, the QTAIM method was first

implemented by Gatti, Saunders and Roetti [16] in the so-called TOPOND program. It adopts the Newton-Raphson algorithm to locate the bond critical points. Derivatives of $\rho(\mathbf{r})$ were approximated by expressing them as linear combinations of Hermite Gaussian functions based on the seminal works of McMurchie and Davison [17] and Saunders. [18] Basin integration, the most costly part of the QTAIM method, is done by an algorithm proposed by Keith [19], representing an improvement over the original work by Biegler-König *et al.* [20]. In Ref. [16], atomic properties of urea were calculated using cluster contains up to 40 atoms. TOPOND includes the Rational Partioned Function of Baker [21] and Banerjee *et al.* [22] as implemented in locating bond critical points by Popelier [23]. Recently, TOPOND has been merged into CRYSTAL14[24] and, taking advantages of its parallel version, has been used in the evaluation of QTAIM properties for systems containing up to 1300 atoms in the unit cell (13000 atomic orbitals). [25]

HI method has been implemented using projector augmented wave (PAW) basis set to study periodic protein clusters as large as 10000 atoms [26]. In 2010, Manz and Sholl [27] proposed a method to evaluate atomic charges that accurately reproduce electrostatic potential for periodic and molecular systems. They also suggested "charge compensation schemes" where atomic reference charges are those of ions calculated with a background density and thus better mimics ions in their natural environment.

The present work documents the original implementation of the HI method in CRYSTAL, a program that computes the electronic structure of periodic systems making use of the Linear Combination of Atomic Orbitals (LCAO) approximation. [24,28]

The manuscript is organized as follows: Sec. 2.1 outlines the implementation of the HI method on periodic LCAO scheme. Computational details of selected examples illustrating different chemical environment are given in Sec. 2.2. The resulting atomic charges compared with Mulliken and QTAIM values are discussed in Sec. 3.1. Finally, the efficiency and numerical accuracy of the implementation are briefly discussed in Sec. 3.2.

2 Methodology

2.1 Periodic HI implementation in Atomic Orbitals basis set

In the periodic LCAO strategy, a basis set of Atomic Orbitals (AO) is considered to span the Crystalline Orbitals (CO) which are in turn the eigenfunctions of one-electron Hamiltonians such as those considered in Hartree-Fock or Kohn-Sham approaches. In a way similar to most molecular codes, the i-th AO in the cell ascribed to lattice vector $\mathbf{g}$, $\chi_i^{\mathbf{g}}(\mathbf{r}) \equiv \chi_i(\mathbf{r}-\mathbf{g})$, is expanded in terms of atom-centered Gaussian-type functions.[28] One of the advantages of the LCAO approximation as implemented in CRYSTAL is that it allows full exploitation of symmetry in practically every step of the calculation.[29] This aspect of the present implementation will be discussed in the following.

Under the LCAO formulation, the Mulliken atomic charge analysis for periodic systems becomes a straightforward extension of the molecular case. This is because the AOs themselves are exploited to partition the electronic structure into atomic contributions. The resulting computational simplicity is probably the reason of

its earliest use in periodic calculations.[1] In addition, thanks to the localized character of the AOs, the density and overlap matrices can be extended just to include contributions from neighbouring cells until they drop off below a given threshold value.[1,18] In practice, this is chosen to maximize saving of memory and cpu time resources and at the same time reaching the desired numerical accuracy.

In the HI scheme, the partition of the total density into atomic constributions is performed by considering suitable functions that weight each point within the spatial region $\mathcal{Q}$ designed as reference cell of the crystal lattice. Such weight functions provide the contributions of each center to the electron density function of the whole system, $\rho(\mathbf{r})$.[9,10] Accordingly, the electronic population assigned to center A, namely N_A, is obtained by means of a spatial integration over $\mathcal{Q}$ of the density times such weight functions according to,

$$N_A = \int_{\mathcal{Q}} d\mathbf{r}\ \rho(\mathbf{r}) w_A(\mathbf{r}), \tag{1}$$

where $w_A(\mathbf{r})$ is the weight function corresponding to the A center.[10]

In terms of the AOs, the periodic electron density reads

$$\rho(\mathbf{r}) = \sum_{i,j} \sum_{\mathbf{g}} P_{ij}^{\mathbf{g}} \sum_{\mathbf{h}} \chi_j^{\mathbf{h}+\mathbf{g}}(\mathbf{r}) \chi_i^{\mathbf{h}}(\mathbf{r}), \tag{2}$$

where $\mathbf{r}$ refers to a given point in region $\mathcal{Q}$ and $P_{ij}^{\mathbf{g}}$ is the density matrix in terms of the AO basis set. In Eq. (2) the translational invariance of both the electron density $\rho(\mathbf{r})$ and the density matrix $P_{ij}^{\mathbf{g}}$ is fully exploited.[1] While the sum is formally infinite with respect to the lattice vector indices $\mathbf{g}$ and $\mathbf{h}$, it is in practice truncated to fulfill a given accuracy threshold using suitable numerical strategies.[1,18,28]

The HI weight function $w_A(\mathbf{r})$ is based on electron densities $\rho_A^{N_A}(\mathbf{r})$ attributed to each isolated center A according to $w_A(\mathbf{r}) = \rho_A^{N_A}(\mathbf{r}) / \sum_{B\in\mathcal{Q}} \rho_B^{N_B}(\mathbf{r})$. [9,10] In the periodic extension of the method, the sum in the denominator is restricted to those centers B located within $\mathcal{Q}$. The domain of the atomic electron density functions is the same region with cyclic boundary conditions. Accordingly, N_A is a given fractional number that corresponds to the atomic population obtained through Eq. (1) in the precedent step along the iterative procedure. [9] To compute the density function ascribed to isolated center A, an atomic density matrix associated to such a fractional occupation number, namely $\mathbf{P}_A^{N_A}$, is built according to

$$\mathbf{P}_A^{N_A} = \mathbf{P}_A^{\mathrm{lint}(N_A)} \left[\mathrm{uint}(N_A) - N_A\right] + \mathbf{P}_A^{\mathrm{uint}(N_A)} \left[N_A - \mathrm{lint}(N_A)\right], \tag{3}$$

where functions uint/lint(N_A) are the upper/lower integers closest to N_A. The density matrix of each center A with integer number of electrons is formulated in terms of the AOs centered on A and they are here obtained from ground state atomic HF-SCF calculations as already implemented in CRYSTAL. [28] The atomic densities $\rho_A^{N_A}(\mathbf{r})$ required to evaluate the weight functions at each point within the cell region $\mathcal{Q}$ are obtained as a particular case of Eq. (2) through

$$\rho_A^{N_A}(\mathbf{r}) = \sum_{ij\in A} \left[P_A^{N_A}\right]_{ij} \sum_{\mathbf{g}} \chi_i^{\mathbf{g}}(\mathbf{r}) \chi_j^{\mathbf{g}}(\mathbf{r}), \tag{4}$$

where now the indices i and j refer to the AOs centered on A. The cyclic condition within region $\mathcal{Q}$ is straightforwardly imposed.

For the numerical integration involved in computation of HI charges, Eq. (1), [9,10] integrands are partitioned within $\mathcal{Q}$ into atomic counterparts considering Voronoi regions multiplied by Becke [7] or Savin [30] weights. In addition, the lattice sums in Eq. (2) are truncated according to particular threshold values.[31] The different atomic parts of the functions are then integrated using radial Gauss-Legendre and angular Lebedev grids.[28] This is the same strategy as implemented in CRYSTAL for numerical integrations of exchange-correlation functionals in periodic Kohn-Sham calculations.[31]

The symmetry properties of each point of the integration grid are estimated as usual in the CRYSTAL code. [29] According to such an analysis, the number of operations that keep a given point invariant or shown it to be equivalent to others are determined consequently. These data are included as additional factors in the above mentioned weights so as to warrant the integration of $\rho(\mathbf{r})$ over $\mathcal{Q}$ to yield the right number of electrons per cell.[31]

With such symmetry adapted weights and irreducible set of points, the integrations corresponding to Eq. (1) are performed as weighted sums along the set. The number of electrons obtained in this way for each center A, namely N'_A, is connected to the actual number of electrons through

$$N_A = \frac{1}{I_A} \sum_q N'_{A_q}, \tag{5}$$

where I_A is the number of point symmetry operators that leave center A invariant and the set $\{A_q\}$ contains all centers in the reference cell equivalent to A by point symmetry operations. The cardinal of the previous set times I_A equals the number of point operations in the space group.

The previously described numerical integration procedure is parallelized in the code by assigning each irreducible set of points an independent task. This allows substantial saving of elapsed computational time as shown in the following.

Our work differs from a previously proposed extension of the HI partition to periodic systems in the context of plane-wave basis sets,[26] in that the efficiency of the present implementation allows all the required data to be generated *on-the-fly* during calculation instead of writing them on disk. This brings about a relevant comparative saving with respect to disk usage and input/output operations.

In the present implementation the iterative procedure normally stops when fulfilling the condition that

$$\left[\frac{1}{N_{\text{total}}} \sum_A \left(N_A^{(i-1)} - N_A^{(i)} \right)^2 \right]^{1/2} < \varepsilon, \tag{6}$$

where N_{total} and $N_A^{(i)}$ are number of atoms and electrons assigned to atom A in the i-th iteration, respectively, and ε is the numerical integration error taken as the absolute difference between computed (fractionary) and actual (integer) total number of electrons. This allows the accuracies of the iterative process and the numerical integrations to be of the same magnitude in final results.

As concerns the use of HI for open-shell systems, it was previously shown [11] that a rigorous application of information theory to the problem involves approaches different than what is here considered for closed-shell cases. As a first

approximation to the issue, in the present work we consider a straightforward extension of the original proposal [9] in which the weight function $\omega_A(\mathbf{r})$ in Eq. (1) is obtained from the total, $\alpha \oplus \beta$, electron density function. The same weight functions are then used to partition the $\alpha \ominus \beta$ spin-density. In this case, one assumes that the physical meaning of the partition in terms of atoms/ions for both densities is mostly contained in the $\alpha \oplus \beta$ electronic distribution. Work is in progress to implement a more rigorous approach that involves a simultaneous 2D fitting of α and β atomic electron densities so as to extend Eq. (3) to the open-shell case as proposed in the FOHI method. [11]

2.2 Computational details

In all calculations here considered, the infinite sums for Coulomb and exchange contributions to the energy are truncated according to five thresholds. They were set to default values of the code unless otherwise specified.[28] QTAIM charges were obtained by means of the TOPOND implementation [32] in CRYSTAL14.[28] The suggested values of nuclear radius, angular planes and radial points have been considered.

The set of illustrative examples includes structures with a variety of periodicity levels (from 0D to 3D) and bonding characteristics (from ionic to covalent). In Table 1 all the compounds are listed, the adopted functionals and basis set are reported (notation Hamiltonian/basis set) and some information on their primitive cells are provided.

Table 1 Structural and computational details of the compounds considered as illustrative tests. NAtoms and NAOs refer to the number of atoms and AOs per primitive cell

		Level of calc.	NAtoms	NAOs
Urea	molecule	PBE/POB-TZVP	8	96
LiPA	polymer	B3LYP/6-31G**	30	294
Cellulose	polymer	PBE/6-31G**	42	516
BN	1-layer	PBE/POB-TZVP	2	36
MgO[Li]	slab	UHF/(see text)	24	212
MgO	crystal	PBE/POB-TZVP	2	37
$SrTiO_3$	crystal	LDA-PZ/(see text)	5	123
α-Al_2O_3	crystal	PBE/(see text)	10	156
Cellulose Iβ	crystal	PBE/6-311G**	84	1032
SALEM-2	crystal	PBE/POB-TZVP	102	1494
α-quartz (SiO_2)	crystal	PBE/POB-TZVP	9	174
α-Fe_2O_3	crystal	(see text)	10	216

Urea continues to be one of the most studied molecules not only due to its chemical, biochemical and physical relevances but also because of it being of great interest in charge density refinement studies. [33] We have calculated the HI atomic charges of urea using the experimental geometry taken from Ref. [33].

The electronic structure of alkali-doped trans-polyacetylenes is interesting since they show markedly increase in conductivity upon doping. [34–36] The polymer undergoes charge transfer from the alkali to the chain which results in formation of geometric solitons [37]. Recently, a charge density analysis of Li-doped trans-polyacetylene (LiPA) has been done by some of us. [38] Periodic calculation at

the B3LYP/6-31G** level showed that, in contrast to Mulliken charges, QTAIM analysis suggests a transfer of almost one electron from the lithium atom to the π-system of the polymer. The results obtained for LiPA (C/Li=7) at the same level of calculation by the three different approaches are shown. The structure and atom labels are schematized in Fig. 1.

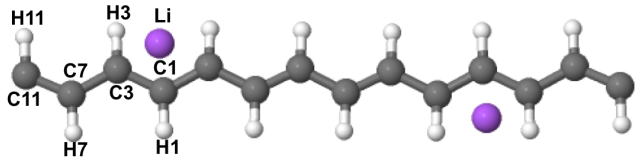

Fig. 1 Schematic representation of the unit cell of Li-Polyacetylene. The atomic charges of labelled atoms are reported in Table 2.

Hexagonal boron nitride is also known as white graphite due to its structural resemblance to that carbon material: layers consist of rings of alternate boron and nitrogen atoms with interplanar interactions including ionic attractions and van der Waals bondings. We have calculated at the PBE/POB-TZVP[39, 40] level the atomic charges of a monolayer slab taken from the bulk structure reported by Hassel. [41]

In introducing the density derived electrostatic and chemical charges, Manz and Sholl [27] calculated the atomic charges of cubic $SrTiO_3$. At the PW91/PAW level they found that the Sr atom lost 2.50 $|e|$ by their own HI implementation. This value is substantially larger than Bader's charge (1.54 $|e|$) and even the formal value for such an element. This result prompted Manz to suggest that HI, at least with the anionic reference densities, overestimates net atomic charges. [42] Vanpoucke *et al.* implementation, on the other hand, shows a lost of only $1.6|e|$ at the LDA/PAW level [43] which is closer to value obtained with QTAIM method. In view of such a controversy, we here include results on the same system computed with the present implementation. As a rather different approach based on AOs basis set is considered, it is interesting to compare them to controversial results obtained with plane-waves. To such a scope we also consider the LDA/PZ [44] functional with a rather large localized basis set. This is similar to that reported by Erba *et al.*, [45] *i.e.* O: 8-411G($2d1f$); Ti: 86-411($2d1f$), while for Sr atom the core pseudopotential and basis set of Heifets *et al.* [46] have been considered.

The Zeolitic Imidazolate Framework SALEM-2[47] [Zn(imidazolate)$_2$] is a Metal-Organic Framework with a Sodalite-like topology closely related to ZIF-8 [Zn(2-methylimidazolate)$_2$].[48] It crystallizes in the $I\bar{4}m$ cubic space group ($a = 16.83$ Å) and exhibits a large pore volume of more than 2400 Å^3 per unit cell. The structure is shown in Fig. 2. The system is here considered as a paradigmatic case of a crystalline system with low density and particular metal-organic interactions, in this case of Zn-N kind.

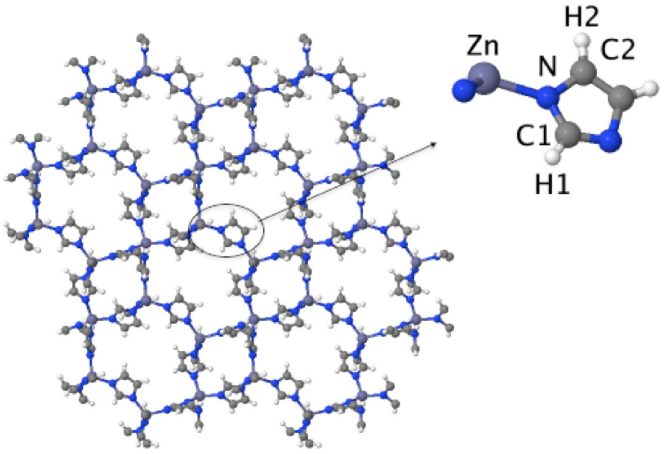

Fig. 2 View of the SALEM-2 Metal Organic Framework, the asymmetric unit is shown on the left and the atom labels refer to data reported in Table 3.

An ionic 3D periodic system, Corundum (α-Al_2O_3), has been also considered as illustrating case. The structure is hexagonal (space group $R\bar{3}c$) and the corresponding cell parameters are $a = 4.76$ Å and $c = 12.99$ Å.[49] The PBE Hamiltonian[39] together with a 8-511G* and 6-31d1 basis set for Al and O, respectively, available in the CRYSTAL web page, [50] have been employed.

Cellulose is the natural bio-polymer most extended in nature, appearing in six different crystalline forms. Concerning the native material, two allomorphs, namely Iα and Iβ, usually coexist in it. As regards the latter, in 2002 Nishiyama *et al.* reported its crystalline structure obtained through very accurate diffraction experiments.[51] Iβ cellulose crystallizes in the monoclinic $P2_1$ symmetry, with 84 atoms per unit cell (42 per primitive cell). The corresponding cell parameters are $a = 7.64$ Å, $b = 8.18$ Å, $c = 10.37$ Å, and $\beta = 96.54°$. The structure and labelling of the atoms in the asymmetric unit are shown in Fig. 3. Calculations have been performed at the PBE level,[39] with the same basis set (standard 6-311G**) and computational conditions as considered in a previous work.[52]

Crystalline MgO is known to be an inert material with a high melting point, consistent with strong ionic bonding, and a wide band gap of 7.8 eV.[53] Its primitive cell contains one formula unit and displays symmetry according to space group $Fm3m$. Owing to its high symmetry and structural simplicity it is a good system for comparisons of computational performances. For the corresponding calculations we have adopted the PBE Hamiltonian[39] with a POB-TZVP basis set.[40] In addition, we have considered a defective slab of MgO, modelled as a three-layers, with a doped Li atom close to an Oxygen vacancy, as shown in Fig. 4. Calculations were performed at the UHF level with a 61-1G [54] basis set for Li and a VDZ one [55] for Mg and O.

We selected the $P3_221$ crystal of α-quartz (SiO_2) as a test case for study[56] because it represents a sort of prototype for an extensively investigated family of

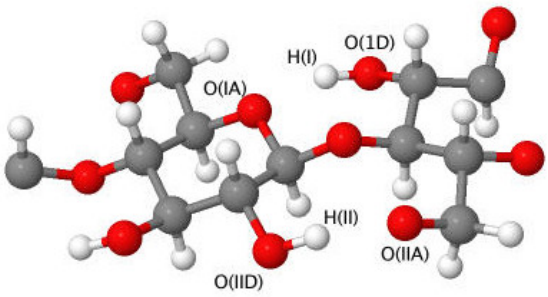

Fig. 3 Schematic view of the β-Cellulose unit cell. Atoms are labelled as belonging to the first (I) and second (II) intra-HB, emphasizing their acceptor (A) and donor (D) features.

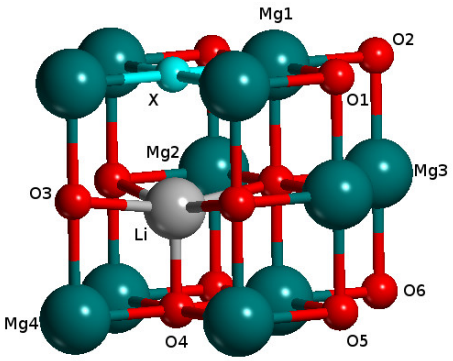

Fig. 4 Unit cell of the Li-doped MgO slab with a Li atom close to an O-vacancy (X). Periodicity is kept along the xy plane and the surface is on top of the draw

silica materials, including zeolites. Calculations were performed at the PBE/POB-TZVP [39,40] computational level.

Hematite (α-Fe_2O_3) is an interesting compound for studying the effect of the Hamiltonian on atomic charges due to the strong correlation between the d-orbital electrons. It is one of the few crystals whose band gap values are commonly used to gauge the level of correlation of the methods.[57] UHF often yields band gaps that are too large, [58] LSDA and SGGA on the other hand give very small or even null band gap. [59] B3LYP [57] gives a band gap of 3.2 eV comparable to the experimental value of 2.0 eV. We have calculated its HI atomic charges and spin-densities for α-Fe_2O_3 with different Hamiltonians, namely UHF, PBE [39] and PBE0 [60] considering 8-6411G* and 8-411G* basis sets [50] for Fe and O, respectively.

3 Results and Discussion

The present implementation will be illustrated in Sec. 3.1 by comparing HI charges with Mulliken and QTAIM ones for the selected set of periodic systems detailed in Sec. 2.2. Results are documented in Tables 2 and 3 in which we also include previous experimental or theoretical data, when available.

Table 2 Atomic Charges calculated with three different partitions of the electron density (Mulliken, HI and QTAIM) for structures periodic in 0 to 2D. When available, results from literature (Lit) are also reported.

System	Atoms	Mulliken	HI	QTAIM	Lit.
Urea (Molecule)	C	0.897	1.100	1.615	1.667[a]
	O	-0.745	-0.669	-1.177	-1.177[a]
	N	-0.463	-1.012	-1.102	-1.214[a]
	H1	0.208	0.390	0.447	0.482[a]
	H2	0.179	0.406	0.437	0.493[a]
LiPA (Polymer)	C1	-0.088	-0.046	-0.124	
	C3	-0.181	-0.469	-0.231	
	C7	-0.064	0.003	-0.020	
	C11	-0.093	-0.158	0.014	
	H1	0.087	0.072	-0.013	
	H3	0.088	0.090	-0.050	
	H7	0.085	0.050	-0.031	
	H11	0.044	0.067	-0.037	
	Li	0.304	0.808	0.900	
Cellulose (fiber)	O(ID)	-0.359	-0.495	-1.059	
	O (IA)	-0.363	-0.256	-1.001	
	H (I)	0.233	0.326	0.594	
	O(IID)	-0.370	-0.495	-1.068	
	O (IIA)	-0.377	-0.495	-1.029	
	H (II)	0.240	0.336	0.582	
BN (Mono Layer)	B	1.259	1.455	2.118	0.429[b]
					1.1[c]
	N	-1.259	-1.455	-2.118	-0.429[b]
					-1.1[c]

[a] Ref. [33]; [b] Ref. [61]; [c] Ref. [62] .

In addition, in Sec. 3.2 data concerning the computational performance of the implemented algorithm are discussed. In particular, its dependence on Hamiltonian (Hartree-Fock or different Kohn-Sham "flavors"), basis set choice, number of symmetry operators and atoms per cell, parallelization and size of the integration grid.

3.1 Illustrating examples

3.1.1 Urea molecule

HI and QTAIM atomic charges for molecular Urea are listed in Table 2 and compared with experimental results. [33] At the first glance it appears that QTAIM charges from both theoretical and experimental density are very similar, with the largest difference being about $0.05|e|$. Notably it is the charge of carbon atom that at the periodic HF/6-31G** level loses $2.54|e|$, see Gatti *et al.*, [16] to be compared to 1.62 (QTAIM theoretical), 1.67 (QTAIM experimental [33]) and $1.1|e|$ (HI). The HI charges are in general smaller than the QTAIM ones for heavy atoms while those of the O and N atoms are comparable to NBO ones calculated at PBE0/cc-pVQZ level reported by Ruedenberg *et al.* [63] The hydrogen atom charges are similar

Table 3 Atomic Charges calculated with three different partitions of the electron density (Mulliken, HI and QTAIM) for 3D systems. When available, results from literature (Lit) are also reported.

System	Atoms	Mulliken	HI	QTAIM	Lit
α-Al_2O_3	Al	2.016	2.485	2.520	
	O	-1.344	-1.656	-1.679	
$SrTiO_3$	Sr	1.275	1.650	1.620	1.62[a]
					2.50[b]
	Ti	1.631	2.240	2.220	2.69[a]
					3.11[b]
	O	-0.968	-1.300	-1.27	-1.43[a]
					-1.87[b]
Cellulose Iβ	O(ID)	-0.439	-0.448	-1.102	
	O (IA)	-0.391	-0.244	-1.004	
	H (I)	0.291	0.330	0.563	
	O(IID)	-0.400	-0.456	-1.104	
	O (IIA)	-0.444	-0.457	-1.114	
	H (II)	0.292	0.331	0.595	
SALEM-2	Zn	0.862	0.667	1.202	
	N	-0.676	-0.383	-1.164	
	C1	0.503	0.250	1.080	
	H1	0.001	0.043	-0.069	
	C2	0.191	-0.006	0.432	
	H2	0.027	0.077	-0.071	

[a] Ref.[43]; [b] Ref.[42].

for HI, QTAIM (theoretical) and QTAIM (experimental). As will be seen below, the Mulliken analysis shows the smallest charge transfer on the average.

3.1.2 Li-doped polyacetylene (Li-PA)

Results reported in Table 2 shows that HI charges are in good agreement with QTAIM ones, as regards the lithium and carbon atoms. In particular, Li loses *ca* 0.8 electrons while C3 is the most charged and C7 is almost neutral (refer to Fig. 1 for atomic labels). On the contrary, charges of hydrogen atoms evaluated with the two methods have opposite sign: each proton loses up to 0.07 $|e|$ considering HI, while it gains an average of 0.03 $|e|$ with QTAIM. However, one is not to put much weight on atomic charges that vary less than $0.1|e|$. These results are somewhat consistent with the observation that QTAIM yields atomic charges slightly larger than HI.[9]

3.1.3 Boron Nitride slab

QTAIM anaysis describes a transfer of more than 2 $|e|$ from B to N while Mulliken and HI methods predict a much smaller transfer of 1.3 and 1.5 $|e|$, respectively. From synchroton data using Maximum Entropy method, Yamamura [62] estimated a transfer of 1.9 $|e|$. The smallest estimation of charge transfer is less than 0.5 $|e|$ from Löwdin analysis of PW91/PAW calculations reported by Topsakal *et al.* [61]

3.1.4 $SrTiO_3$

Our HI and QTAIM results for the Sr, Ti and O atomic charges are documented in Table 3 together with Mulliken charges for comparison. According to the comment provided in Sec. 2.2, these are in quite good agreement with those reported by Vanpoucke *et al.*, [43] even considering a radically different implementation. This confirms that HI charges for this periodic system are similar to QTAIM, which differs significantly from Manz and Sholl [27,42] findings.

3.1.5 Corundum (α-Al_2O_3)

Atomic charges for this system and the following ones are collected in Table 3. Although some degree of electron back-donation from O to Al atoms is expected for this ionic crystal, Mulliken charges overestimate the effect providing a charge transfer of $\approx 1|e|$ per Al atom. The ionic character of this oxide is revealed by both the HI and QTAIM analysis in which the back-donation phenomenon is substantially less relevant.

3.1.6 Cellulose Iβ

Results for both the isolated chain and the 3D arrangement are tabulated in Tables 2 and 3, respectively. Two different intra-molecular hydrogen bonds (HB) are presented in the unit cell, labelled I and II; see Fig. 3. As usual, each HB is characterized by an O atom acting as the donor (D) and the other as acceptor (A). As a general trend, isolated chain displays a charge on O atoms slightly larger than in the crystalline structure. In fact, as polymers arrange to constitute the crystal, additional interchain HBs appear yielding a decrease of the O atom charges. In this respect, it is worth noting that, while both QTAIM and HI exhibit a similar trend, Mulliken points to the opposite effect.

3.1.7 Metal-organic framework (SALEM-2)

At variance with previously studied cases, in SALEM-2 the three partitions of the electron density here exhibit a rather different behavior. QTAIM analysis, see Table 3, provides a much more ionic picture than Mulliken and HI and, rather unexpectedly, it assigns a charge larger than the formal one to the Zn atom. HI and Mulliken charges are qualitatively more similar to each other but, in contrast with previously studied cases, Mulliken predicts a more ionic system than HI. It is suspected that the zero-flux surface surrounding the zinc atomic basin is too flat and thus might have contributed to the uncertainty of the integrated atomic charges in the QTAIM case. Nonetheless the discrepancy between Mulliken and HI suggests that a bond of particular characteristics between Zn and N atoms is occurring. These surprising results deserve a more detailed study which is beyond the scope of the present work.

3.1.8 MgO[Li] slab with Oxygen vacancy

The open-shell implementation is illustrated through a surface defect represented by a 2D slab whose reference cell is in a doublet spin state. The structure is

electrically neutral as the charge deficiency connected with the substitution of a Mg^{2+} by a Li^{+} is compensated by an isolated electron in the O vacancy. The latter, labeled as X in Fig. 4, is described by a dummy atom with the same O basis set. The atomic charges and spin-densities of the symmetry irreducible atoms are reported in Table 4.

Table 4 UHF atomic charges and spin-densities for a three-layers slab of MgO doped with a Li atom close to an O vacancy (see Fig. 4).

	Mulliken	HI	QTAIM
Li	0.990 (0.000)	1.031 (0.000)	0.917 (0.000)
Mg1	1.936 (0.016)	2.013 (0.018)	1.800 (0.030)
Mg2	1.973 (0.000)	2.060 (0.000)	1.808 (0.000)
Mg3	1.959 (0.000)	2.053 (0.000)	1.799 (0.000)
Mg4	1.964 (0.000)	2.041 (0.000)	1.821 (0.000)
X	-1.002 (0.892)	-1.026 (0.784)	-0.880 (0.773)
O1	-1.959 (0.013)	-2.069 (0.051)	-1.820 (0.035)
O2	-1.967 (0.000)	-2.053 (0.000)	-1.828 (0.000)
O3	-1.949 (0.004)	-2.018 (0.010)	-1.771 (0.009)
O4	-1.948 (0.000)	-2.026 (0.000)	-1.779 (0.000)
O5	-1.955 (0.000)	-2.034 (0.000)	-1.782 (0.000)
O6	-1.955 (0.000)	-2.036 (0.000)	-1.819 (0.000)

All three methods show similiar trends for both atomic charges and spin-densities. It is interesting noting that in this case, the HI method depicts a slightly more ionic distribution than the other two methods. The unpaired electrons appear to localize mainly on the defect site X with a small contribution of the spin-density from the neighboring atoms.

3.1.9 Correlation Analysis

The present set of data allows us to perform a statistical analysis similar to that provided in a previous work on the performance of HI for neutral molecules.[9] In that case, the correlation between HI charges and those obtained using other electron density analyses was carried out. The analysis here undertaken just consider Mulliken and QTAIM for comparison and a more modest sample size: 13 periodic systems against 168 molecules.[9] In addition, the correlation for molecules mostly included non-metallic elements, namely C, H, N, O, F and Cl, which appear predominantly bonded in a covalent way to each other. On the contrary, many of the systems considered here display ionic or semi-ionic bonding character together with covalent ones. This is because their composition includes not only non-metallic but also different metal and transition metal elements. Accordingly, results are not expected to exhibit a neat correspondence between both sets of data. Nonetheless, this would give a rough idea on how differently the performances of HI for periodic and molecular systems do compare.

The three atomic charge analyses here considered, namely Mulliken, QTAIM and HI, show a rather consistent tendency. We have performed a linear fit analysis of the 70 atomic charges reported in Tables 2, 3, 4, 5 and 9. The regression equation for the Mulliken vs. HI charges is $(0.8270x - 0.0307)$ and for the QTAIM vs. HI charges is $(0.9356x - 0.0266)$. The first observation is that the HI charge is more

consistent with the Mulliken one ($R^2 = 0.9404$) than it is with the QTAIM charge ($R^2 = 0.9139$). The slopes of both functions are smaller than unity which shows that HI charge is consistently larger than Mulliken charge but smaller than QTAIM one. However, despite the poorer correlation, the general trend of HI appears to be more similar to QTAIM than Mulliken, as the corresponding slope is closer to unity. Figure 5 shows that both lines intersect closely with the origin since sample systems are all neutral.

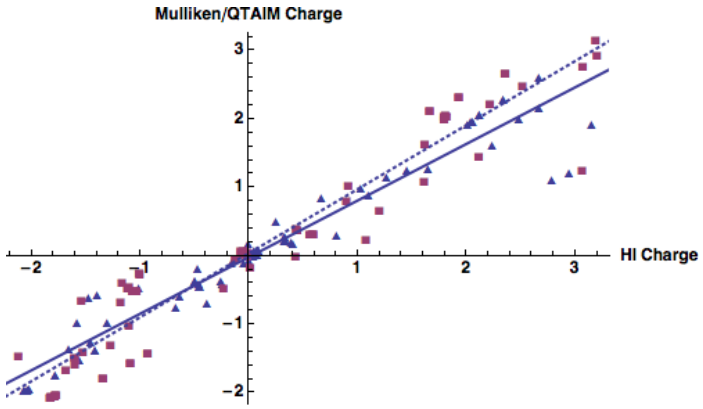

Fig. 5 Linear fit for HI vs. Mulliken charges (solid line, triangles) and HI vs. QTAIM charges (dotted line, squares).

When the H, C and O atoms are analyzed separately, the correlations between the HI and Mulliken charges, for example, deteriorate unevenly. The corresponding values are $R^2 = 0.7799$, 0.8765, 0.8556, respectively. This implies that the correlations of the metal elements, again between the HI and Mulliken charges, are significantly better than for electronegative ones.

The present correlation analysis between HI and Mulliken charges contrasts with that previously reported for neutral molecules.[9] In that work, a substantially poorer agreement between both charge analyses ($R^2 = 0.17$) arised. Such a difference is to be mostly attributed to the fact that the elements that supposedly prevail in the sampling set of molecules are actually in the first row of the periodic table. As previously shown, they display the worst correlation between both methods.

3.2 Computational performance

3.2.1 Effect of Basis Set

As in the molecular case, the choice of basis set is of great importance to the accuracy in calculations for periodic systems. This is in particular due to the large number of bond types existing in such a kind of systems. Plane waves and localized basis functions are popular schemes implemented. Plane wave basis sets are not dependent on neither atomic type nor atomic positions, they are BSSE free

but instead exhibit Pulay stress owing to their dependence on unit cell size and shape.[64] Their computational implementation is much simpler than for localized functions. On the other hand, the latter set requires a much smaller number of basis functions to adequately describe void and atomic core regions. Concerning the latter, it is worth noting that there is no need to consider pseudo-potentials as in the plane-wave case. Additionally, properties such as projected density of states or atomic charges are comparatively more straightforward. Ideas of basis sets that work well for molecular systems, for example the case of diffuse functions, may not transfer well to periodic systems.[65] In fact, problems associated with diffuse functions lead to the development of the POB-TZVP and POB-DZVP basis sets that are tailored to solid-state calculations by Peintinger, Oliveira and Bredow[40] where, beside being smaller than the starting Ahlrichs def2-TZVP basis, [66,67] gaussians with orbital coefficients smaller than 0.1 were removed (with exception for certain metals where the basis is then designated as POB-TZVP+(s,p)) which helps relieve linear dependency.

In Table 5 we have tabulated the atomic charges of α-Quartz and Hematite, calculated at PBE and PBE0 levels, respectively, with Mulliken, HI and QTAIM. Calculations for Hematite have been performed with the $\{6, 6, 6, 7, 13\}$ set of parameters for integrals calculations. Four different basis sets were considered in each case which are detailed in Table 5. Basis set labeled BS1 is a split-valence triple-ζ one specially optimized for Hematite.[58]

Concerning α-Quartz, the trend exhibited as increasing the variational flexibility of basis set reflects what is expected from previous results on molecules.[9] In fact, at variance with Mulliken, HI charges monotonically approach QTAIM values in going from minimal to triple-ζ basis set level as it arises from results listed in Table 5.

Table 5 Basis set effect on atomic charges computed under different charge partition approaches: α-Quartz and Hematite cases.

Approach	Atom	STO-6G	6-31G** [a]/BS1[b]	POB-DZVP	POB-TZVP
			α-Quartz (SiO_2)		
Mulliken	Si	1.150	1.125	1.221	1.930
	O	-0.575	-0.562	-0.611	-0.965
HI	Si	1.268	2.787	2.947	3.154
	O	-0.634	-1.394	-1.474	-1.577
QTAIM	Si	3.068	3.074	3.203	3.191
	O	-1.538	-1.524	-1.602	-1.597
			Hematite (α-Fe_2O_3)		
Mulliken	Fe	0.644	2.285	1.799	1.365
	O	-0.429	-1.523	-1.199	-0.910
HI	Fe	0.727	2.340	1.259	1.173
	O	-0.485	-1.560	-0.840	-0.782
QTAIM	Fe	2.292	1.934	1.925	1.924
	O	-1.301	-1.089	-1.086	-1.079

[a] α-Quartz. [b] Hematite.

On the contrary, charges for Hematite exhibit a much more erratic behavior. According to the SCF energy trend, the variational flexibility order for the considered basis sets is STO-6G < POB-DZVP < BS1 $\lesssim$ POB-TZVP. It arises from data supplied in Table 5 that QTAIM analysis provides as usual atomic charges

practically independent of the basis set choice, at least as regards the four richest sets. On the contrary, both Mulliken and HI schemes yield an extremal charge separation in the BS1 case, unexpectedly suggesting a larger ionicity than QTAIM. In general, it appears that the trend displayed by Mulliken and HI is very similar, a fact that reflects a significant basis set dependency in the latter.

From the chemical point of view, the difference between both considered systems is the cationic element involved, namely Si or Fe. It is likely that the basis set erratic behavior of Mulliken and HI charges is connected to the appearance of unfilled d orbitals in the latter.

3.2.2 CPU time dependence on computational conditions

We now turn to the comparative computational cost of HI and QTAIM. This is illustrated in the following four systems with different periodicity: Urea (0D), Li-PA (1D), BN monolayer (2D) and Corundum (3D). The corresponding CPU times are detailed in Table 6.

Table 6 CPU time (in s) of HI and QTAIM for Urea molecule, LiPA, BN monolalyer and Corundum (α-Al_2O_3).

	Urea (mol)	Li-PA (pol)	BN (slab)	α-Al_2O_3
HI	16	22	23	14
QTAIM	4565	7559	2249	6576

The results show that in this implementation, HI calculation is more than two orders of magnitude faster than QTAIM one while yields comparable atomic charges. Though such calculations are substantially more costly than Mulliken ones they are still fast in comparison to an electronic structure calculation. As examples, for two medium size systems like Li-PA and SALEM-2, the ratio between the whole SCF and HI parts of the calculation is 38 and 30, respectively. It is worth noting that the cost of the HI calculation is due largely to the integration in Eq. (1) and thus depends on the unit cell and grid sizes. Comparing with the numerical integration, calculation of atomic density matrix in Eq. (3) is insignificant. These aspects will be further discussed in Sec. 3.2.3.

In Sec. 2.1 the exploitation of symmetry equivalences in the costly numerical integration step has been discussed. We have calculated the HI charges for the MgO supercell ($2 \times 2 \times 2$) in which the number of point symmetry operations is systematically reduced from 48 to 1. The dependence of the CPU time on this number of symmetry operators is shown in Fig. 6.

It appears that the computational time roughly decreases as $1/N_{\mathcal{G}}$, $N_{\mathcal{G}}$ being the number of point symmetry operators in space group $\mathcal{G}$. This behavior is based on the fact that the number of symmetry irreducible points of the grid (where the electron density and weight functions are actually evaluated for integration) roughly scales as the total number of points divided by $N_{\mathcal{G}}$.

We have also employed the MgO system to study the CPU time dependence on the unit cell size. Several supercells of this system have been considered and the different CPU times of different supercells and grid sizes are shown in Table 7.

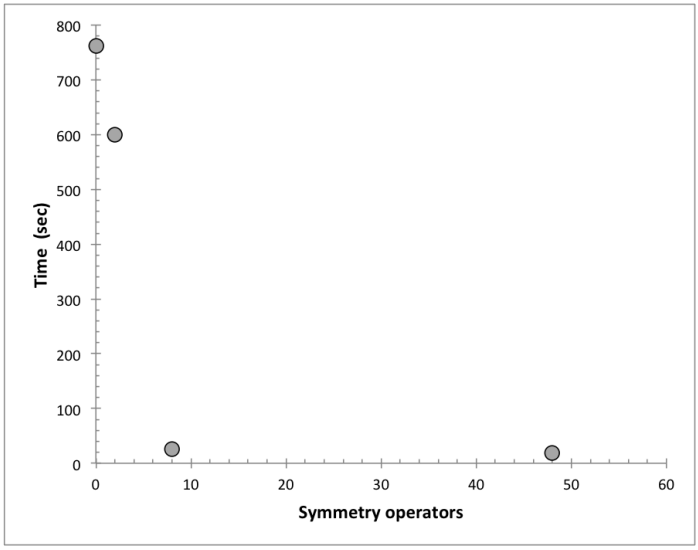

Fig. 6 CPU time dependence on number of symmetry operators. MgO supercell $2 \times 2 \times 2$

Table 7 Dependence of CPU time on unit cell size in terms of number of atoms per unit cell (N At/u. c.) and number of symmetry irreducible points in the integration grid (N Grid Pts). Severa MgO supercells are considered.

N At/u. c.	N Grid Pts	CPU Time (sec)
2	747	1.6
8	1507	4.8
16	2679	13.1
32	4678	15.4
64	9330	27.5

It turns out that the computational time increases with the number of atoms in the unit cell in a proportion similar to that due to the number of symmetry irreducible points in the integration grid.

A rather large supercell ($5 \times 5 \times 5$) of the same system with 250 atoms and 4625 AOs per cell has been considered to illustrate the performance of parallel implementation described in Sec. 2.1. A quite dense grid has been considered in this case, namely a pruned (75,974) one (see Sec. 3.2.3 for notation). The dependence of the elapsed time on the reciprocal of the number of processors ($1/N_{\mathrm{procs}},\ N_{\mathrm{procs}} \in \{64, 32, 16, 8, 4, 2\}$) is shown in Fig. 7.

Figure shows that for values of $1/N_{\mathrm{procs}} > 1/32 = 0.03125$ the behavior of elapsed time is close to linear, refecting an efficient task distribution among processors and the absence of time consuming operations like input/output ones. As the number of threads increases to 64, the trend clearly loses the linear character suggesting that non-parallelized parts of the algorithm start to take relevance in the computational cost. These are principally the definition and classification of the grid points and the calculation of the atomic density matrices considered in Eq. (4) at each iteration. Additionally, the communication between processors is partially responsible of such a slight efficiency decay.

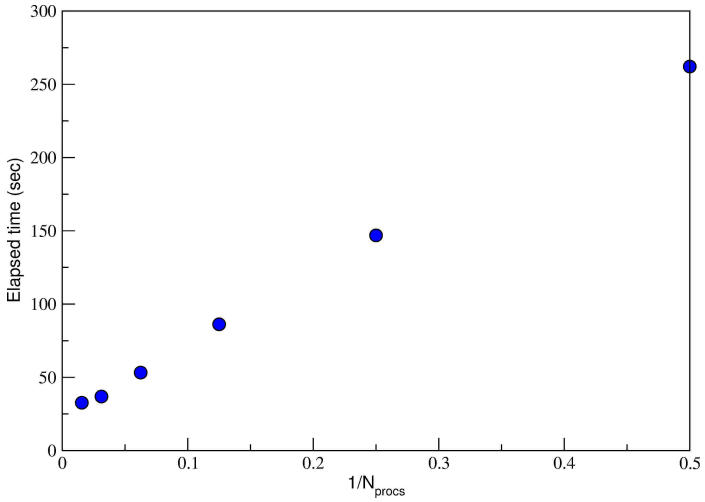

Fig. 7 CPU time of parallel calculations in dependence on the reciprocal of the number of processors ($1/N_{\mathrm{procs}}$) for MgO supercell ($5 \times 5 \times 5$).

3.2.3 The influence of the integration grid density on accuracy and timing

In the present implementation, it is possible to set by input the accuracy of the numerical integration in Eq. (1). Four different predefined grids are available which are collected in Table 8 together with the corresponding number of symmetry irreducible points for the α-Quartz case (see Sec. 2.2). The considered grids are pruned and here denoted as (r, a), where r and a are the number of radial and maximum number of angular points, respectively. [28,31] The computational cost of the HI calculation together with the integration accuracy, evaluated as the absolute difference between numerically integrated and actual number of electrons per unit cell are also tabulated.

Table 8 α-Quartz. Different integration grids *vs* CPU time (sec) and accuracy in total number of electrons ($|e|$)

Grid	N points	CPU Time	Accur
(55,434)	9738	109	2×10^{-4}
(75,434)	21459	114	1×10^{-4}
(75,974)	44267	219	6×10^{-5}
(99,1454)	87416	453	1×10^{-5}

An estimation of the accuracy in the determination of atomic charges is the previously defined integration accuracy divided by the number of atoms, Eq. (6). In the case of α-Quartz with 9 atoms per unit cell, it turns out that even with the less dense grid, namely (55,434), the accuracy *per* atomic charge is about 10^{-5} which is in general enough for most applications. Such a grid is the default for the HI implementation in CRYSTAL and it was considered in most of the illustrating examples. Computational cost of integration in such conditions is more than four times faster than the cost with the largest grid (99,1454).

3.2.4 The Hamiltonian choice

In Table 9 Mulliken, HI and QTAIM atomic charges together with the corresponding spin densities for antiferromagnetic α-Fe_2O_3 calculated at the UHF, PBE0 and PBE levels, are listed. Calculations were performed under the same computational conditions as considered in Sec. 3.2.1. Charges corresponding to PBE0 are listed in Table 5 and also here for the sake of easy comparison.

Table 9 Hamiltonian effect on Hematite (α-Fe_2O_3) atomic charges and absolute values of the spin-densities (in brackets)

	Fe			O		
	PBE	PBE0	UHF	PBE	PBE0	UHF
Mulliken	2.059	2.285	2.618	-1.373	-1.523	-1.746
	(3.689)	(4.290)	(4.740)	(0.000)	(0.001)	(0.000)
H-I	2.120	2.340	2.669	-1.413	-1.560	-1.779
	(3.496)	(4.070)	(4.504)	(0.000)	(0.001)	(0.000)
QTAIM	1.666	1.934	2.361	-0.929	-1.089	-1.340
	(3.620)	(4.209)	(4.652)	(0.001)	(0.001)	(0.001)

Ionicity increases in passing from PBE to UHF descriptions of the system while PBE0 atomic charges are in between, a fact that somehow reflects the ability of this hybrid method to better recover the experimental band gap values. The spin-densities on Fe atoms display a somehow parallel trend. The values obtained with Mulliken and HI partitions indicate that in all cases the electronic structure appear to be much more ionic when considering the latter analysis, but at the same time the spin densities are smaller. The enhancement of the ionicity of the system respect to QTAIM featured by HI is the largest one with PBE and decreases as increasing the contribution of the exact exchange in calculations.

4 Conclusions

The present work describes an implementation for the extension of the molecular HI method to periodic electronic structures. Its particularity with respect to other periodic implementations [11,26,42,43] is that it is suitable for both Hartree-Fock and Kohn-Sham wave-functions spanned in terms of a basis set of AOs. The method was implemented in the CRYSTAL code and its performance is here illustrated by several examples.

The HI atomic charges obtained through this implementation have been compared with Mulliken and QTAIM ones in several test cases that cover different bonding types and periodicity levels. In most of them it turns out that, as it has been also found for molecules, [9] Mulliken tends to provide charges substantially smaller in absolute value than QTAIM, but HI provides intermediate values in general closer to the latter than to Mulliken, an effect that becomes more significant as increasing the size of the AO basis set. Such a general behavior however exhibits exceptions as, for instance, the Metal-Organic Framework SALEM-2.

The present implementation exploits in a great part the machinery already implemented in the CRYSTAL code for the numerical integration of the different

quantities employed in Kohn-Sham calculations. Notably is the exploitation of symmetry equivalences that allows the computation of the HI charges for systems as large as the above mentioned SALEM-2 with a primitive cell volume of 2490 $Å^3$ and 102 atoms in barely 22 s of CPU time. Using the same machine the cost of the whole energy calculation in direct mode is 663 s. Additionally it is shown that the implementation scales linearly with the unit cell size, it is easily paralellized, and its computational efficiency allows avoiding input/output operations generating all required quantities *on-the-fly* in each iteration.

Acknowledgements CMZW and AMNL acknowledge financial support from Mexican CONACyT through project CB-178853. AMNL thanks a posdoctoral grant from "Red de Fisicoquímica Teórica" (CONACyT project # 253498).

References

1. C. Pisani, R. Dovesi, C. Roetti, *Hartree-Fock Ab Initio Treatment of Crystalline Solids*, *Lecture Notes in Chemistry Series*, vol. 48 (Springer, Berlin, 1988)
2. R.S. Mulliken, J. Chem. Phys. **23**(10), 1833 (1955)
3. P.O. Löwdin, Adv. Quantum Chem. **5**, 185 (1970)
4. A.E. Reed, R.B. Weinstock, F. Weinhold, J. Chem. Phys. **83**, 735 (1985)
5. A.J. Stone, M. Alderton, Mol. Phys. **56**, 1047 (1985)
6. F.M. Bickelhaupt, N. Hommes, C.F. Guerra, E.J. Baerends, Organometallics **15**(13), 2923 (1996)
7. A. Becke, J. Chem. Phys. **88**, 2547 (1988)
8. R.F.W. Bader, *Atoms in molecules. A quantum theory* (Clarendon, Oxford, 1990)
9. P. Bultinck, C. Van Alsenoy, P.W. Ayers, R. Carbó-Dorca, J. Chem. Phys. **126**, 144111 (2007)
10. F.L. Hirshfeld, Theor Chim Acta **44**, 129 (1977)
11. D. Geldof, A. Krishtal, F. Blockhuys, C. Van Alsenoy, J. Chem. Theory Comput. **7**, 1328 (2011)
12. J.F. Harrison, Theor Chim Acta **133**, 1486 (2014)
13. T.C. Lillestolen, R.J. Wheatley, J. Chem. Phys. **131**, 144101 (2009)
14. T. Verstraelen, P.W. Ayers, V. Van Speybroeck, M. Waroquier, Chem. Phys. Lett. **545**, 138 (2012)
15. A.J. Misquitta, A.J. Stone, F. Fazeli, J. Chem. Theory Comput. **10**, 5405 (2014)
16. C. Gatti, V.R. Saunders, C. Roetti, J. Chem. Phys. **101**(12), 10686 (1994)
17. L.E. McMurchie, E.R. Davidson, J. Comput. Phys. **26**(218) (1978)
18. V.R. Saunders, Faraday Symp. Chem. Soc. **19**, 79 (1984)
19. T.A. Keith, Molecules in magnetic fields. Ph.D. thesis, MacMaster University, Hamilton, ON Canada (1993)
20. W.F. Biegler-König, R.F.W. Bader, T.H. Tang, J. Comput. Chem. **13**, 317 (1982)
21. J. Baker, J. Comput. Chem. **7**, 385 (1986)
22. A. Banerjee, N. Adams, J. Simons, R. Shepard, J. Chem. Phys. **89**, 52 (1985)
23. P. Popelier, Chem. Phys. Lett. **228**, 160 (1994)
24. R. Dovesi, R. Orlando, A. Erba, C.M. Zicovich-Wilson, B. Civalleri, S. Casassa, L. Maschio, M. Ferrabone, M.D.L. Pierre, P. D'Arco, Y. Noël, M. Causà, M. Rérat, B. Kirtman, Int. J. Quantum Chem. **114**, 1287 (2014). DOI: 10.1002/qua.24658
25. S. Casassa, A. Erba, J. Baima, R. Orlando, J. Comp. Chem. **36**, 1940 (2015)
26. D.E.P. Vanpoucke, P. Bultinck, I. Van Driessche, J. Comput. Chem. **34**(5), 405 (2012)
27. T.A. Manz, D.S. Sholl, J. Chem. Theory Comp. **6**, 2455 (2010)
28. R. Dovesi, V.R. Saunders, C. Roetti, R. Orlando, C.M. Zicovich-Wilson, F. Pascale, B. Civalleri, K. Doll, N.M. Harrison, I.J. Bush, P.D. Arco, M. Llunell, M. Causà, Y. Nöel, *CRYSTAL14 Users Manual* (University of Turin, Turin, 2014)
29. R. Orlando, M.D.L. Pierre, C.M. Zicovich-Wilson, A. Erba, R. Dovesi, J. Chem. Phys. **141**, 104108 (2014)
30. A. Savin, Int. J. Quantum Chem. **S22**, 457 (1988)
31. M.D. Towler, A. Zupan, M. Causà, Comp. Phys. Comm. **98**, 181 (1996)

32. C. Gatti, S. Casassa, Topond14 user's manual. CNR–CSRSRC. Milano, Italia (2014)
33. H. Birkedal, D. Madsen, R.H. Mathiesen, K. Knudsen, H.P. Weber, P. Pattison, D. Schwarzenbach, Acta Crys. A **60**(5), 371 (2004)
34. J. Tsukamoto, A. Takahashi, K. Kawasaki, Jpn. J. App. Phys. Part 1 **29**(1), 125 (1990). DOI 10.1143/JJAP.29.125
35. Y. Cao, P. Smith, A.J. Heeger, Polymer **32**, 1210 (1991)
36. T. Schimmel, W. Reiss, J. Gmeiner, M. Schworer, H. Naarmann, N. Theophilou, Solid State Commun. **65**, 1311 (1988)
37. W.P. Su, J.R. Schrieffer, A. Heeger, Phys. Rev. B **22**, 2099 (1980)
38. M. Ho, A.M. Navarrete-López, C.M. Zicovich-Wilson, A. Ramírez-Solís, J. Phys. Chem. B **117**(2), 725 (2013)
39. J.P. Perdew, Y. Wang, Phys. Rev. B **45**, 13244 (1992)
40. M.F. Peintinger, D.V. Oliveira, T. Bredow, J. Comput. Chem. **34**(6), 451 (2013)
41. O. Hassel, Norsk Geologisk Tidsskrift **9**, 266 (1927)
42. T.A. Manz, J. Comp. Chem. **34**, 418 (2013)
43. D.E.P. Vanpoucke, I.V. Driessche, P. Bultinck, J. Comp. Chem. **34**, 422 (2013)
44. J.P. Perdew, A. Zunger, Phys. Rev. B **23**, 5048 (1981)
45. A. Erba, K.E. El-Kelany, M. Ferrero, I. Baraille, M. Rérat, Phys. Rev. B **88**, 035102 (2013)
46. E. Heifets, E.A. Kotomin, A.A. Bagaturyants, J. Maier, J. Chem. Phys. Lett. **6**, 2847 (2015)
47. O. Karagiaridi, M.B. Lalonde, W. Bury, A.A. Sarjeant, O.K. Farha, J. Am. Chem. Soc. **134**, 18790 (2012)
48. K.S. Park, Z. Ni, A.P. Cote, J.Y. Choi, R. Huang, F.J. Uribe-Romo, H.K. Chae, M. O'Keeffe, O.M. Yaghi, Proc. Natl. Acad. Sci. U. S. A. **103**, 10186 (2006)
49. J. Lewis, D. Schwarzenbach, H.D. Flack, Acta Crystallogr., Sect. A **38**, 733 (1982)
50. The CRYSTAL Web Page. URL http://www.crystal.unito.it/
51. Y. Nishiyama, P. Langan, H. Chanzy, J. Amer. Chem. Soc. **124**(31), 9074 (2002)
52. A.M. Navarrete-López, M.L. San-Román, C.M. Zicovich-Wilson, Theor. Chem. Acc. (2016). DOI: 10.1007/s00214-016-1889-6
53. S.H. Tamboli, R.B. Patil, S.V. Kamat, V. Puri, R.K. Puri, J. Alloys Compd. **477**, 855 (2009)
54. R. Dovesi, E. Ermondi, E. Ferrero, C. Pisani, C. Roetti, Phys. Rev. B **29**, 3591 (1983)
55. M. Causà, R. Dovesi, C. Pisani, C. Roetti, Phys. Rev. B **33**, 1308 (1986)
56. B. Civalleri, P. D'Arco, R. Orlando, V.R. Saunders, R. Dovesi, Chem. Phys. Lett. **348**, 131 (2001)
57. E.A. Moore, Phys. Rev. B **76**, 195107 (2007)
58. M. Catti, G. Valerio, R. Dovesi, Phys. Rev. B **51**, 7441 (1994)
59. P.J. Punkkinen, W.H. K. Kokko, I.J. Väryynen, J. Phys.: Condens. Matter **11**, 2341 (1999)
60. C. Adamo, V. Barone, J. Chem. Phys. **110**, 6158 (1999)
61. M. Topsakal, E. Akturk, S. Ciraci, Phys. Rev. B **79**(11), 115442 (2009)
62. S. Yamamura, M. Takata, M. Sakata, J. Phys. Chem. Solids **58**(2), 177 (1997)
63. A.C. West, S.M. W., M.S. Gordon, K. Ruedenberg, J. Phys. Chem. A **119**, 10368 (2015)
64. G. Francis, M. Payne, J. Phys.-Cond. Mat. **2**(19), 4395 (1990)
65. A. Gruneich, B.A. Heb, Theor. Chem. Acc. **100**, 253 (1998)
66. F.Weigend, F. Furche, R. Ahlrichs, J. Chem. Phys. **119**, 12753 (2003)
67. F.Weigend, R. Ahlrichs, Phys. Chem. Chem. Phys. **7**, 3297 (2005)